OFFICE OF NAVAL RESEARCH

Contract No. N00014-91-J-1409

Technical Report No. 149

Charge-Dependent Atomic-Scale Structures of High-Index and (110) Gold Electrode Surfaces as Revealed by Scanning Tunneling Microscopy

by

Xiaoping Gao, Gregory J. Edens, Antoinette Hamelin , and Michael J. Weaver

Prepared for Publication

in

Surface Science

Department of Chemistry

Purdue University

West Lafayette, Indiana 47907-1393

February 1994

ABSTRACT

The atomic and nanoscale structures of high-index gold surfaces in aqueous perchloric acid electrolyte as revealed by in-situ scanning tunneling microscopy (STM) under electrode potential control are reported with the objective of ascertaining systematically the terrace-step morphology and superstructures as a function of the crystallographic orientation. Six faces, Au(221), (331), (533), (311), (210), and (410), two each lying in the three fcc crystallographic zones, were selected to investigate the role of the step orientation and terrace width for non-vicinal faces. Data for the low-index surface Au(110) are also included for comparison with Au(331) and (221), since all three feature formally a n(111)-(111) terrace-step structure. Measurements of the double-layer capacitance as a function of the electrode potential, E, in dilute (10 mM) perchloric acid were also undertaken in order to evaluate the potential of zero charge (E_{pzc}) for each surface and to check the potential-dependent surface stability. The two surfaces in the (111)-(100) zone, Au(533) and (311), both display essentially (1 × 1) (i.e bulk-termination) atomic structures at positive electrode charges (i.e. for $E > E_{pzc}$), yet exhibit significant surface relaxation at negative charges involving edge-atom depression and row buckling. For the surfaces in the (111)-(110) zone, Au(221) and (331), however, such surface relaxation is seen even at positive electrode charges. This behavioral difference can be understood on the basis of the differing step structures present in the two zones. Moreover, Au(331) undergoes a reversible (1 × 2) reconstruction at negative charges, involving row pairing. This reconstruction is compared with that for Au(110), which also involves "row pairing" but for which a variety of local microstructures can be observed. The faces in the (100)-(110) zone, Au(210) and (410), exhibit locally ordered atomic arrangements indicative of an essentially bulk-termination structure, although only the former yields discernably ordered steps. The longer-range superstructures, specifically involving domain-edge propagation across monoatomic steps, exhibit systematic trends consistent with the presence of an effectively *attractive* step-step interaction at distances within ca 5 Å.

1. INTRODUCTION

The remarkably direct experimental access to the real-space atomic structure of ordered metal surfaces that can now be provided by scanning tunneling microscopy (STM) is exerting an increasingly substantial influence on our understanding of electrochemical as well as ultrahigh vacuum (uhv) interfacial systems[1]. For the former type, an emphasis has been placed so far on gold low-index surfaces. This interest arises in part from the chemical and electrochemical inertness of gold, allowing the surface structure to be examined by in-situ STM over wide ranges of electrode potential (and surface electronic charges) in the virtual absence of faradaic processes. Moreover, such studies have demonstrated that all three low-index gold faces undergo reconstruction at negative (or near-zero) electrode charges, which is removed at positive charges[2-6]. Remarkably detailed corroboration of these findings has been provided by surface X-ray scattering measurements[7-10]. The reconstructions observed in the aqueous electrochemical environments match well the structures obtained (or proposed) for the clean gold surfaces in uhv. Besides the acquisition of detailed surface atomic arrangements, STM has proved to be a valuable probe of the nanoscale structural rearrangements attending the potential-induced formation and removal of the reconstruction[2b,5b,11-13].

Given this favorable situation for the low-index faces, it is of considerable interest to explore the atomic- and nanoscale structure and stability of higher-index (or stepped) gold surfaces, lying in crystallographic zones between the low-index faces. Despite the practical as well as fundamental importance of such surfaces, there is a severe paucity of STM examinations along these lines in uhv[14-18] as well as in electrochemical environments[19-21]. One contributing factor is the difficulty in obtaining *true* atomic-resolution images for such highly corrugated surfaces[20]. Nevertheless, STM can be anticipated

to provide much-needed information concerning the local atomic and nanoscale structure of stepped surfaces.

As part of a concerted effort devoted to the elucidation of atomic-level structure and dynamics at ordered gold-aqueous interfaces by means of in-situ STM, we have examined the substrate structures for a number of faces located in the $[\bar{1}10]$, $[0\bar{1}1]$, and [001] [i.e. the (111)-(110), (111)-(100), and (100)-(110)] zones. A preliminary report of some of our findings, specifically concerning potential-induced surface relaxation, appeared recently[20]. We have selected for detailed study six such surfaces, two in each of the three crystallographic zones. These faces: Au(221), (331), (533), (311), (210), and (410), are mostly located close to zone "turning points", so that the terraces separating the (anticipated) monatomic steps are expected to be narrow, consisting of four or fewer gold atoms[22]. (The location of these faces in the fcc stereographic triangle, along with unit-cell ball models for the bulk-terminated structures, is summarized for the convenience of the reader in Fig. 1.) Pertinent results are described in the present report. Of particular interest is the manner and degree to which such densely stepped surfaces undergo relaxation and possibly reconstruction, following earlier observations of such phenomena for Au(311), (533), and (221)[20].

With these results and additional data for the other three faces now in hand, we focus here on the dependence of the observed surface restructuring upon the crystallographic orientation which emerges upon intercomparing the behavior of neighboring faces both within and across the crystallographic zones. An additional component of this study, also presented below, concerns a possible relationship between the potential-induced restructuring and the electrochemical double-layer properties[23], involving the hysteresis observed for capacitance-potential responses in the vicinity of the potential of zero charge (E_{pzc})

depending on the direction of the potential sweep. While we are concerned here chiefly with densely stepped faces, we describe briefly the terrace structure of a vicinal face, Au(554). We also report further on the nature of the potential-induced reconstruction on Au(110), described earlier in preliminary form[4], and its relationship to the closely allied stepped face Au(331).

2. EXPERIMENTAL SECTION

Most details of the experimental in-situ STM protocol are available in earlier reports[2,12]. The microscope is a Nanoscope II (Digital Instruments) equipped with a bipotentiostat for electrochemical STM. The STM tips were 0.01 inch tungsten wire etched electrochemically in 1 M KOH. All STM images were obtained in the so-called "height mode", i.e. at constant tunneling current, and are displayed here chiefly *without* electronic filtering. This current was typically 10-20 nA, and the tip-substrate bias voltage was in the range ± 10 to 100 mV. The gold crystals (hemispheres, 5 mm diameter) were prepared by AH at LEI-CNRS. They were pretreated, as before[2,12,20] by flame annealing, cooled in ultrapure water, and transferred to the STM cell containing 0.1 M $HClO_4$, protected by a drop of water. The counter and reference electrodes were gold wires, the latter being electrooxidized prior to use so to yield an approximately poised potential in 0.1 M $HClO_4$. All electrode potentials quoted here, however, are versus the saturated calomel electrode (SCE).

The double layer capacitance-potential (C_{dl}-E) data were obtained in a conventional electrochemical cell with a reversible hydrogen electrode (RHE) as the reference electrode. The latter measurements employed a 5 mV ac signal (13 to 115 Hz) with phase-sensitive detection using a PAR Model 5204 lock-in amplifier, with a PAR 173/179 potentiostat. Only partial positive-feedback iR compensation was applied, so to avoid the possibility of potential instability

and ensuing damage to the gold crystal surface. The E-dependent C_{dl} values were extracted from the quadrature and in-phase components in the usual manner. The perchloric acid was double-distilled grade (G.F. Smith) and the water was purified by means of a "Milli-Q Plus" system (Millipore).

3. RESULTS

We first present pertinent STM results for the high-index surfaces examined here, alongside a briefer summary of the atomic-scale findings from our earlier study for Au(533), (311), and (221) together with some additional data. We now consider the structural results for faces within the $[\bar{1}10]$, $[0\bar{1}1]$, and [001] zones, and then Au(110), in turn.

3.1 *Au(331), (221), and (554)*

The stepped faces along the $[\bar{1}10]$ zone are of interest in part because they are expected to consist of terraces having (111) orientation separated by (111) steps (Fig. 1). Thus the terminating face along this zone, Au(110), can be designated as 2(111)-(111) in the terrace-step notation of Lang et al[22]. This face reconstructs in electrochemical as well as uhv environments to the well-known "missing-row" configurations having (1 × 2) [and (1 × n)] symmetries[4,6,9]. The proximity of the Au(331) face, which can be designated equivalently as 3(111)-(111) or 2(111)-(110), invites the question of whether a related reconstruction can be obtained for this surface. Relatively little experimental information is available for (331) metal surfaces[24].

Figure 2A shows a typical unfiltered STM image, displayed in a 30° off-normal (height-shaded) representation, of a large (16 nm square) region of the Au(331) crystal in 0.1 M $HClO_4$ at 0.2 V vs. SCE. This potential corresponds to a small positive electronic charge. (Values of E_{pzc} for this and the other surfaces studied in the present work are presented and discussed below.) Evident

in Fig. 2A are uniformly ordered gold atomic rows running diagonally. A close-up of a ca 6 nm square region towards the top right-hand corner of Fig. 2B is shown to facilitate observation of some atomic-scale features. Clearly discernable are steps and parallel strings of metal atoms. The measured interatomic spacing along the rows is 2.9 (± 0.2) Å, consistent with the known gold atomic diameter of 2.89 Å. Within a given domain, featuring adjacent terrace strings separated by monoatomic steps, the measured unit-cell distance perpendicular to the strings is 6.3 (± 0.3) Å, close to the value (6.14 Å) expected for the ideal bulk-termination structure. Only two atomic rows are discernable within each unit cell in this direction, rather than the three expected for each (111) terrace facet. This is not surprising, however, since the third row should be located partly beneath the terrace step.

Given that the 3-atom wide (111) terraces should be tilted by 22° from the (331) surface plane, one might expect that the z-corrugation of the juxtaposed terrace atomic strings would be significantly different, enabling the slant direction to be ascertained directly from the STM images. Such a corrugation is not clearly evident, however, from Figs. 2A and B. Nevertheless, such information can be gleaned from the geometry of monatomic domain edges lying in the path of the terrace strings. Several such steps are located, for example, in the middle of the imaged area in Fig. 2B. The added rows, located towards the upper part of the image, are seen to be shifted to the left of the underlying atomic strings. Given that one would expect that such rows would add preferentially to the "foot" of the terrace, below each terrace edge, this observation enables us to ascertain that the (1 × 1) terrace plane is slanted downwards (diagonally) from left to right in the images shown in Figs. 2A and B.

Interestingly, however, the left-hand atomic string within each unit cell, while expected to be higher in the (331) plane, actually appears to be slightly

lower (i.e. "less bright", smaller z displacement) in Fig. 2. We interpret this observation as indicating the occurrence of surface relaxation*, with the terrace-edge (left-hand) atomic row being depressed relative to the adjacent terrace row. Such surface relaxation, shown schematically in ball-model form in Fig. 3A, is qualitatively consistent with theoretical predictions and some experimental observations[25]. The extent of such relaxation, at least as inferred from the STM z-corrugation, is quite marked, in that the terrace-edge atom appears to be about 0.2 Å lower than the adjacent terrace atom. A portion of this observed effect could arise from an electron-tunneling artifact, associated with structure-driven spatial variations in the local electronic density of states. The observation of significant deviations in the x-y atomic positions from the (1 × 1) structure, however, suggest strongly that *some* surface relaxation is occurring.

In addition to such "distorted (1 × 1)" *domains*, surface regions on Au(331) were encountered which feature microfacets containing more than two terrace atom rows between each step. Such a region is present towards the top left-hand corner of Fig. 2A. Evident are terrace segments containing at least three juxtaposed atomic rows, thereby being equivalent to (221) facets. Terraces consisting of even four or five (111) oriented atomic rows were also occasionally observed.

Adjusting the electrode potential to values negative of E_{pzc} (−0.05 V, vide infra), however, yielded a pronounced change in the Au(331) surface structure.

---

* We utilize the term "surface relaxation" in the present paper to denote shifting of top-layer atoms away from the (1 × 1) (bulk termination) structure without significant alteration in the unit-cell symmetry. The term "surface reconstruction" is reserved for atomic rearrangements where clearcut alterations in the unit-cell geometry are observed.

Figure 4A displays a large-scale (50 nm square) region of Au(331) imaged shortly after altering the potential to −0.3 V. Parallel rows of steps along the [1$\bar{1}$0] direction are still clearly evident (although running in a diagonally different direction compared with Fig. 2 due to a different crystal x-y orientation in the microscope). Closer inspection, as exemplified in the 15 nm square image shown in Fig. 4B, reveals a "paired-row" structure: while the interatomic spacing along the rows remains 2.9(± 0.2) Å, the distance between the double-row partners is 4.0 (± 0.3) Å, the separation between each "unit-cell" pair being 12.5 (± 0.4) Å, [i.e. twice the step spacing in the essentially (1 × 1) geometry discussed above]. We can therefore designate this modified structure as having (1 × 2) symmetry. Furthermore, the atomic positioning along each string is such that a line drawn through nearest-neighbor atoms in adjacent rows is essentially 90° (± 4°) to the [1$\bar{1}$0] direction. While it is difficult to discern atomic detail in the troughs between each row pair (and virtually impossible in the half-tone published images!), the measured z-corrugation between the tunneling maxima (i.e. gold atomic row members) and the adjacent trough is about 0.6 (± 0.2) Å. The presence of significant interaction within the row pairs is signaled by the observation of small (even undetectable) z corrugation between the atomic rows, suggestive of electronic delocalization. (This situation is similar to that encountered in STM images for hexagonal reconstructed Au(100)[2c].) The internal structure of the row pairs, including the row separation (4.0 Å), is similar to that anticipated (and found) for the unreconstructed Au(110) surface. This potential-induced (1 × 1) → (1 × 2) structural transformation was found to be reversed rapidly (largely within a few seconds) upon altering the potential back to values, ca 0.2–0.3 V, significantly above E_{pzc}.

The likely nature of the row pairing, giving rise to the (1 × 2) structure,

is shown schematically in Fig. 3B. We envisage that alternate rows of initially terrace-edge atoms, labelled "1" in the ideal bulk-termination structure shown in Fig. 3B, can move by one lattice spacing to the left (as shown), so to "pair" with the adjacent unchanged terrace-edge row, located 4 Å away. An alternate (and mechanistically more likely) transformation entails atom 1 moving into the position occupied by the atom initially at the foot of the terrace step, with the latter atom simultaneously shifting into site 4. (Both these alternative atomic rearrangements are indicated with arrows in Fig. 3B.) Regardless of the precise mechanism, some relaxation of the second-layer gold atoms is also expected. Unlike the (1 × 1) → (1 × 2) "missing-row" reconstruction of Au(110), only short-range atomic motion is evidently necessary to form the Au(331)-(1 × 2) structure.

The other instructive feature of the potential-dependent STM images obtained for Au(331) concerns the longer-range superstructures, especially the propagation of domain edges running across the $[1\bar{1}0]$ strings. The large-scale image of the (1 × 1) structure (Fig. 2A) shows the presence of numerous kinks along the $[1\bar{1}0]$ direction, formed by a distinctly random termination of individual microterrace rows. That is, there is little coherence in the location of these microdomain edges as one proceeds across the strings. This observation suggests the presence of little or no interaction between the neighboring $[1\bar{1}0]$ rows, similarly to the Au(110) (1 × 2) surface as observed by STM in uhv[26].

Interestingly, however, the formation of the Au(331)-(1 × 2) structure is accompanied by a significant change in the morphology of these microdomain edges, as can be discerned readily in Fig. 4A. The termination of the paired-row strings is seen to occur largely coherently across the $[1\bar{1}0]$ direction, so that fewer and less extended kinks are evident than in the (1 × 1) structure (Fig. 2A). This property of the (1 × 2) lattice is consistent with the observed tendency to produce uniform (1 × 2) structures even close to domain edges, in

that the individual rows are constrained to terminate in nearby locations along the [1$\bar{1}$0] direction in order to facilitate the degree of row pairing.

Summarized in our preliminary report[20] are atomic-resolution STM data for Au(221) in aqueous 0.1 M $HClO_4$. The bulk-termination structure for this face, designated 4(111)-(111), features one more atomic row across each (111) microterrace than is the case for unreconstructed Au(331) (Fig. 1). At positive electrode charges, the Au(221) surface displays a similarly relaxed structure as for Au(331). This point is evident in the atomic-scale image shown in Fig. 5A. Ordered atomic strings are observed, again lying along the [1$\bar{1}$0] direction, with three adjacent atomic rows being discernable within each unit cell, the center string being the brightest. Using the same tactics as described above for Au(331), the left-side member of each trio of rows is nonetheless deduced to constitute the "terrace-edge" in the (1 × 1) structure. Again, the observation of an apparent z-depression of this row compared with the adjacent center-terrace row is indicative of significant or even substantial surface relaxation. The presence of an additional atomic row between terrace steps for Au(221) compared with Au(331) is, of course, expected on the basis of their (1 × 1) structures.

In contrast to Au(331), however, the Au(221) surface does not undergo clearcut reconstruction at negative electrode charges, the (1 × 1), albeit relaxed, atomic structure being maintained under these conditions. [Indeed, the image for Au(221) in Fig. 5A was obtained below E_{pzc}, at −0.2 V.] Another, possibly related, difference between Au(221) and Au(331) concerns the morphology of the domain edges. Figure 5B is a large-scale (25 nm square) image of a typical region on Au(221) in 0.1 M $HClO_4$ at 0 V. Evident is a high density of extended kinks formed across the [1$\bar{1}$0] direction. While a quantitative judgment is difficult, the density of such kinks appears to be higher than for Au(331) under conditions where the relaxed (1 × 1) structures are present for both

surfaces (i.e. at positive electrode charges). This observation is consistent with the smaller interaction between adjacent terrace rows on Au(221) than on \u(331) anticipated from the longer distance between terrace steps for the former (ca 8.5 Å versus 6.1 Å).

A more cursory examination was also made of a vicinal face, Au(554), which also lies in the [$\bar{1}$10] zone but close to the (111) pole: this surface can be designated as 10(111)-(111). Well-ordered (111) terrace regions were observed, with monoatomic steps along the [1$\bar{1}$0] direction as anticipated from the bulk-termination structure. The spacing between the step, however, was not entirely uniform, terrace widths as narrow as 5-6 atoms and as wide as 20-30 atoms being observed.

3.2 Au(311) and (533)

Both surfaces lying within the [0$\bar{1}$1] zone that are included in the present study, Au(311) and Au(533), were discussed in our preliminary report[20]. In apparent contrast to Au(331) and (221), these surfaces yield atomic-resolution STM images at positive electrode charges with terrace-step structures displaying z-corrugations that approximate those expected for the bulk-termination (1 × 1) surfaces. At negative electrode charges, however, relaxed structures were apparent that feature edge-atom depression in a similar fashion to those discussed above. For Au(311), which can be designated equivalently as 2(111)-(100) or 2(100)-(111), only the terrace-edge atomic rows are discernable at positive electrode charges. Below E_{pzc}, however, both atomic rows within each (111) [or (100)] terrace string between the monatomic steps are imaged with comparable intensity, compatible with the occurrence of surface relaxation[20] (see Fig. 1 of ref. 20).

Unlike Au(331), the Au(311) surface displays ordered domain edges cutting

across the [1$\bar{1}$0] direction at positive as well as negative electrode charges. (Several such domain edges are discernable in Figs. 1a-c of ref. 20.) Such coherent domain-edge superstructures, which are commonly observed for low-index gold surfaces [e.g. Au(100), ref. 12], are indicative of significant interactions between adjacent terrace steps, as for reconstructed Au(331) (vide supra).

The Au(533) surface, designated as 4(111)-(100), also undergoes a related surface relaxation below E_{pzc}. Similarly to Au(221), trios of atomic strings were observed along the [1$\bar{1}$0] direction, with the terrace-edge atomic row apparently being depressed sufficiently so that the adjacent row on the (111) terrace appears brighter, thus inferring a higher z-coordinate[20]. A difference with Au(221), however, is that the Au(533) structure incurs a significant xy relaxation[20]. As might be expected from the foregoing, the Au(533) surface displays largely random extended kinks across the [1$\bar{1}$0] direction, indicative of little or no interaction between adjacent monoatomic steps. A typical large-scale image displaying such superstructures is shown in Fig. 6, which was obtained at 0.2 V. Similar domain-edge patterns persisted when the potential was altered to and from values above and below E_{pzc}.

3.3 Au(210) and (410)

An interesting characteristic of faces in the third, [001], zone is that the surface coordination number of the top-layer atoms is relatively low, resulting from the "open" nature of the constituent (100) and (110) poles. The Au(210) face, designated 2(100)-(110) or 2(110)-(100), is of some interest as it forms the turning point in this zone. The minimum distance between top-layer atoms in the Au(210)-(1 × 1) structure is 4.08 Å [i.e. equal to the separation between the rows in Au(110)-(1 × 1)], with the interatomic spacing across the [001] direction being 5.0 Å. The other surface in the [001] zone examined here,

Au(410), designated 4(100)-(110), thereby features a longer interatomic spacing, 8.5 Å, between the (110) steps.

Figure 7A shows a large-scale (23 nm square) image of Au(210) in 0.1 M $HClO_4$ obtained at 0 V. While some short-range (< 10 nm) atomic order is evident, the surface exhibits longer-range disordering in the z direction, i.e. no consistent flat domains were observed. The close-up (9 nm square) image shown in Fig. 7B shows more detail of the degree of atomic ordering that can be observed. At least in some regions, near-uniform atomic spacings are observed that, moreover, yield interatomic distances and angles that match well the bulk-termination structure. (In both Figs. 7A and B, the near-vertical rows correspond to the [001] direction.) Interestingly, there is no evidence of restructuring in that the regions where atomic order is maintained consistently exhibit (1 × 1) patterns. Essentially the same structural arrangements were observed throughout the potential range −0.4 V to 0.3 V, corresponding to both negative and positive electrode charges.

Partly similar results were obtained for Au(410). A typical large-scale (16 nm square) image, obtained at −0.1 V is shown in Fig. 8. While the surface exhibits distinct long-range z-disordering, at least some local atomic ordering is again discernable. The observed atomic pattern, however, while consistent with an approximately (1 × 1) structure, arises chiefly from (100) terrace atoms. The additional observation of ordered (110) steps, so to yield a complete (1 × 1) pattern, is limited typically to a few small (< 1-2 nm) surface regions.

3.4 Au(110)

While Au(110) is formally a low-index face, it is instructive to consider the potential-dependent structural behavior given that this surface should be highly corrugated. Moreover, the behavior of Au(110), which can be considered

to be 2(111)–(111), is of interest given the nature of the potential-induced reconstruction observed for the nearby stepped face, Au(331) (vide supra). While we have reported some preliminary STM observations of the potential-induced reconstruction on Au(110) in perchloric acid electrolytes[4], it is appropriate to consider here some findings from a more detailed ensuing study. (Further details will be available in a separate report[31].) An interesting in-situ STM study of this system, albeit without true atomic-resolution detail, was also reported recently by Magnussen et al[6].

Figure 9A shows a typical large-scale (ca 30 nm square) region of Au(111) in 0.1 M $HClO_4$ after altering the potential to a value, -0.3 V, where surface reconstruction is prevalent[4]. Clearly discernable are dense arrays of parallel strings, running in the $[1\bar{1}0]$ direction. Vestiges of terrace steps running across these strings can also be seen, although there is little coherence between the termination points of adjacent strings (cf ref. 26). (Images of the (1 × 1) structure, stable at positive charge densities[26], on the other hand exhibit relatively well-ordered domain edges across the $[1\bar{1}0]$ direction, similarly to Au(311).) In regions close to such (former) terrace edges, the lower-terrace strings tend to be packed more tightly. The closest adjacent strings are separated by 8.2 (± 0.3) Å, which would correspond to a (1 × 2 structure). Prominent, however, are a range of larger string separations, especially that (ca 16.5 Å) corresponding to a (1 × 3) structure. Also of interest is the observed z–x STM corrugations across the strings. For the (1 × 2) case, the maximum corrugations (i.e. the z-displacement between adjacent atomic maxima and minima) is about 0.7 Å. For larger inter-string separations [i.e. for (1 × n), where n > 2] larger z corrugations, 1.2–1.7 Å, are generally obtained.

Atomic-resolution STM images of such reconstructed regions show that these apparent variations in row heights (and also in row widths) are associated with

the presence of several distinct string microstructures. A close-up image illustrating this point, obtained in the same experiment as Fig. 9A, is shown in Fig. 9B. In addition to the variations in string separation, at least two distinct atomic row structures are evident in Fig. 9B. The first, seen most clearly towards the right-hand edge of the image, consists of a near-symmetrical trio of gold atoms, with the center string having the highest z-displacement. This type of microstructure is that usually proposed for the so-called "missing-row" (110) reconstruction. The second, more prevalent, string arrangement seen in Fig. 9B, however, consists of a *duo* of monatomic rows. While the atomic positions between the row pairs are staggered, they are shifted by only ca 10-15° from an essentially "square planar" packing arrangement. Several other short-range mutations of these string microstructures are also seen in Fig. 9B.

Surface regions were also observed that feature similar large-scale variations in string morphologies, yet contain more uniform row atomic structures. An example is shown in Figs. 10A and B. The former is a large-scale image displaying similar string superstructures as in Fig. 9A. The close-up (atomic-resolution) image, Fig. 10B, shows essentially uniform and symmetrical strings consisting of trios of gold rows. The set of strings in the right-hand side of Fig. 10B exhibit a clearcut (1 × 2) unit cell, whereas the pair on the left-hand side constitute a local (1 × 3) arrangement. Similarly to reconstructed Au(331), the row pairing seen on Au(110) is typically characterized by weak z-corrugations between the individual atomic rows, again suggestive of electronic delocalization.

While such symmetrical "missing-row" (or "added-row") arrangements can be observed repeatedly, the partial or even dominant presence of other string microstructures (such as in Fig. 9B) is a notable characteristic of this surface. Emphasized in our preliminary communication on Au(110)[4] are asymmetric (1 × 2)

microstructures that apparently feature significant distortions in the x-y packing of top-layer atomic rows. Further examples of the structural varieties that are repeatedly observed by STM are shown in the atomic-resolution images in Fig. 11 A and B. An instructive feature of Fig. 11A is the presence of an interrupted but otherwise well-ordered string (situated in the middle-left of the imaged region). The interrupted segment, while missing the center atomic string, still displays an adjacent pair of atoms. This structural arrangement suggests that the atomic-row trio is actually formed by the addition of a *single* center atomic row, together with a relaxation of the outer pair of rows so to yield the observed three-atom wide string. Figure 11B displays a relatively uniform, yet further distinct, row structure consisting of row pairs overlaid on a relaxed (1 × 3) arrangement.

At least a qualitative picture of the metal mass transport associated with the development of such reconstructions can be gleaned from the above results. While the formation of ordered (1 × 2) arrays necessarily would involve long-range mass transport, at least on large terraces, it is apparent that only more local atomic motion may well be involved. As is well known, the production of (1 × 3) structures can be envisaged to occur by means of short-range row pairing. While "clustered" islands of (1 × 2) structure are commonly seen (cf ref. 6), considerably more "open" regions are also prevalent (Figs. 9A, 10A), so that the average atomic density commonly approaches that for the (1 × 3) structure. Short-range atomic motion, again yielding local "added-" as well as "missing-row" regions, is also often observed near terrace edges lying across the $[1\bar{1}0]$ direction. The very inhomogeneous nature of the reconstructed surface therefore allows large changes in *local* atomic density to occur without requiring longer-range mass transport.

Noteworthy in the present context is that the basic nature of the atomic

"row-pairing" observed for Au(110) is closely related to the form of reconstructed Au(331). The relationships between the potential-dependent atomic structures for the various surfaces examined here are discussed below.

3.5 Comparison with Capacitance-Potential Measurements

The STM results presented above show clearly that the manner and degree to which the surface atomic (and nanoscale) structure depends upon the electrode potential varies markedly with the crystallographic orientation. Nevertheless, while surface relaxation is evident for most ordered high-index faces, only Au(331) is seen to undergo a clearcut potential-dependent *reconstruction*, i.e. involving substantial x-y reorganization of the surface atoms. As already noted, the occurrence of surface reconstruction at least at negative electrode charges is now well established for all three low-index gold faces[2-13]. The original suggestion of this phenomenon, which predated the in-situ microscopic (as well as ex-situ[27]) measurements, was based on the observation of hysteresis in potentiodynamic double-layer measurements[28]. More specifically, a.c. capacitance-potential (or voltammetric current-potential) curves for low-index gold electrodes can display noticeable and even marked dependences on the direction of the potential sweep and the potential range accessed[23,28,29]. These effects are now known to be due at least partly to the occurrence of potential-induced reconstruction whereby the surface structural changes associated with its formation and removal yield some degree of electrochemical irreversibility. The comparison between such electrochemical data and potential-induced changes in local microscopic structure as probed by STM has been pursued in greatest detail for the Au(100) surface, for which the atomic structural rearrangement is very marked[11,12,30]. One might expect that this approach would also be instructive for other surfaces displaying potential-dependent

structures, such as the present high-index surfaces as well as Au(110) and (111).

To this end, capacitance-potential (C_{dl}-E) data were obtained for each gold face studied here, over potential ranges (within the region ca -0.4 V to 0.7 V) that span those where the STM structural data were acquired. More dilute, 10 mM, perchloric acid electrolyte was utilized in order to discern also the value of E_{pzc} from the characteristic diffuse-layer C_{dl}-E minimum, E_{min}, observed under such conditions. Figures 12A-C summarize typical C_{dl}-E data obtained during positive- or negative-going potential sweeps at 5 mV s^{-1}, for faces lying in the $[\bar{1}10]$, $[0\bar{1}1]$, and [001] zones, respectively. Included where appropriate are corresponding data for the Au(110) and (111) surfaces.

We found no detectable hysteresis in the C_{dl}-E curves for the majority of high-index faces, namely Au(221), (311), (533), (210), and (410), in that the positive- and negative-going potential traces are *precisely* superimposed. Interestingly, however, the Au(331) [and Au(110)] faces display significant hysteresis (Fig. 12A). Thus, the E_{min} values obtained during positive-going sweeps from -0.35 V are significantly more positive than for negative-going sweeps, by about 25 mV and 10-15 mV for Au(331) and (110), respectively. (Slightly different hysteretic behavior for Au(110) was shown under some conditions in an earlier report[29b](e.g. Fig. 4b), probably due to surface contamination.) Holding the potential at the negative limit, -0.35 V, for periods up to 10 min also has little effect on the ensuing positive-going C_{dl}-E curves. The hysteresis is observed to propagate from potentials just below E_{pzc} to about 0.3 V and 0.6 V for Au(331) and (110), respectively. A similar hysteresis is also seen for Au(111) (Fig. 12B).

For the high-index gold surfaces which are seen by STM to undergo little or no potential-induced structural changes, or surface relaxation (as opposed to marked reconstruction), the double-layer properties are entirely reversible with

respect to potential alterations under these conditions. Irreversibility in the potential-dependent double-layer structure is only therefore evident for the Au(331) surface [along with Au(110) and (111)], which are seen to incur clearcut potential-induced surface reconstruction.

Given the stable and well-defined E_{min} values which are obtained for most of the present surfaces, since E_{min} can essentially be identified with E_{pzc} (in dilute nonadsorbing electrolytes) it is worthwhile to consider briefly the observed dependence of E_{min} upon the crystallographic orientation. Correlation between E_{pzc} for different gold crystallographic orientations and various independent interfacial parameters, especially the estimated surface free energy or the density of "broken bonds", d_{bb} (related to the average surface coordination number[32]), have been examined by several authors[23,33,34]. However, a reason for reexamining this point here is that most earlier E_{pzc} values were obtained in fluoride electrolytes, where the likelihood of incipient surface oxidation at even small positive charges obliges the use of positive-going potential sweeps when evaluating E_{min}, enhancing the possibility that surface reconstruction will affect E_{pzc} and hence E_{min}. A plot of E_{min} for the various gold faces considered here versus the crystallographic orientation [expressed as the angle versus the (110) pole] is shown in Fig. 13. The continuous trace also shown in Fig. 13 refers to the d_{bb} value (left-hand y axis), estimated in the manner outlined in ref. 32. As described earlier [23,33], in order to examine the correlation between E_{min} and d_{bb} it is desirable to "scale" the axes by selecting a pair of faces for which the d_{bb}-crystallographic angle curve is forced to coincide with E_{min}.

The two surfaces selected for this purpose in Fig. 13 are Au(111) and (110) since these low-index faces exhibit extreme d_{bb} (and E_{min}) values. A complication is that both surfaces exhibit potential-dependent reconstruction and, moreover,

the (111) surface yields E_{min} values in perchloric acid media that are significantly (50–100 mV) lower than in the nonadsorbing electrolyte KPF_6 [35], also being sensitive to the electrode history and the electrolyte concentration*[36]. The E_{min} value for Au(111) chosen here, 0.3 V, was obtained in KPF_6 electrolyte[35]. The E_{min} value for Au(110) [and for Au(331)] used in Fig. 13 refers to the negative-going potential sweep (Fig. 12 A,C) since the bulk-termination (1 × 1) structure is more likely to be approached for this condition. Also included in Fig. 13 is a E_{min} value for Au(100); this was also obtained in 10 mM $HClO_4$ during a negative-going potential sweep, under conditions where an ordered (1 × 1) surface structure is known to predominate[37].

Inspection of Fig. 13 shows that a reasonable correlation is achieved between d_{bb} and E_{min} for most high- as well as low-index gold faces on this basis. This observation is similar to that reached in ref. 23 and 33.

4. DISCUSSION

4.1 *Charge-Dependent Atomic Structures*

Combined with our preliminary report[20], the STM results presented above demonstrate strikingly the ordered nature of most of the high-index gold surfaces with respect to the atomic spacing and uniformity of the steps as well as the terraces. Nevertheless, significant and even substantial departures from the ideal (1 × 1) "bulk termination" structures are observed which invite rationalization and interpretation. Compared with the low-index "flat terraced"

---

* This behavior may be due in part to the role of steps and other imperfections as well as the occurrence of slight perchlorate specific adsorption: the former should exert a particularly large influence in diminishing the work function (and hence E_{pzc}) on the (111) surface in view of the smooth hexagonally close-packed nature of the terraces.

surfaces (111) and (100), the structural characteristics of high-index surfaces provoke additional interesting questions. Not all the surface atoms on stepped faces are equivalent. Some of these atoms, such as those at step sites, feature a high density of "broken bonds" (i.e. have a lower surface coordination number). While the distances between such step rows may well be large (several atomic diameters or more), the effects of longer-range interactions between steps can be evident in the superstructure morphology. Moreover, the forces acting upon the top-layer atoms will not necessarily be balanced in the x-y direction due to the structural symmetry of high-index faces. The systematic atomic-level structural information for the surface charge-dependent structures for the various high-index faces now in hand can offer at least qualitative insight into the controlling physical factors.

The behavioral comparison of surfaces in the $[\bar{1}10]$ and $[0\bar{1}1]$ zones is of interest since these faces can usefully be considered in most cases to consist of (111) terraces separated by (111) and (100) steps, respectively. One difference noted immediately between the pairs of $[\bar{1}10]$ faces studied here, (331) and (221), compared with the $[0\bar{1}1]$ faces, (311) and (533), is that only the latter pair exhibit essentially (1 × 1) (bulk termination) structures at positive electrode charges. Both the former surfaces appear to undergo significant surface relaxation under these conditions, involving depression of the terrace-edge atoms and a coupled motion of neighboring atoms (Fig. 3A). While a qualitatively similar form of surface relaxation is also observed for (311) and (533), this is only achieved at negative electrode charges.

A simple rationalization of these behavioral differences is suggested from the ball-model structures shown in Fig. 1. While surfaces in both the $[\bar{1}10]$ and $[0\bar{1}1]$ zones feature (111) oriented terraces, the (111) orientation of the steps for the former orients the step rows at a different angle to the terrace atoms

than is the case for the (100) steps present in the latter zone. For the former, relaxation of the step atoms diagonally downwards (in the manner shown in Fig. 3A) would involve these atoms shifting (formally) from a threefold to bridging site with respect to the underlying lattice. For the latter, however, this relaxation would involve a shift from a threefold to a near-atop site. On this (albeit oversimplified) basis, then, one would expect the former, $[\bar{1}10]$, faces to more readily undergo surface relaxation than the latter, $[0\bar{1}1]$, faces, in accordance with the STM observations.

A second property of the present surfaces which varies markedly with the crystallographic orientation concerns the domain-edge superstructures. Comparison between the related stepped faces Au(311) and (533), which have the same terrace-step structure yet exhibit different distances (4.9 and 8.6 Å, respectively) across the steps, is instructive in that only the former surface displays coherent domain edges, i.e. does not form extended kinks along the $[1\bar{1}0]$ direction. Meandering domain edges similar to Au(533) are also observed for Au(221) and (331) in the absence of reconstruction, for which the step-step distances are greater than 6 Å, whereas more coherent domain edges are seen for the unreconstructed Au(110) surface, for which the corresponding distance is only 4.1 Å.

This behavior suggests that step rows separated by less than ca 5 Å can display significant net *attraction* between each other, so that domain edges cutting across the $[1\bar{1}0]$ direction tend to propagate uniformly rather than form kinks. The presence of *repulsive* interactions between step rows on high-index surfaces, arising from elastic strain and dipolar forces, has been discussed extensively recently in connection with step roughening, i.e. the formation of kinks directed *across* the step direction [e.g. refs 38-40]. To our knowledge, however, the present evidence for an attractive step-step interaction over a

range, $\lesssim$ 5 Å. longer than the usual cohesive-bond distances has not been gathered previously. The underlying reasons for such a relatively long-range attraction are not obvious to us, although one can surmise the presence of though-bond propagation of cohesive energy, involving underlying as well as top-layer atoms.

The observation of at least short-range ordered (1 × 1) structures for Au(210) is also of some significance, given that the top-layer metal atoms are somewhat "isolated", being separated by 4.1 and 5.0 Å along and across the [001] direction, respectively. No evidence for a "missing-row" (1 × 2) structure for this face, predicted theoretically[41], was obtained here. Not unexpectedly, however, "roughening" in the z-direction prevails in that no coherent domain edges are evident and the x-y ordered regions are relatively small, < 10 nm. The very limited propagation of ordered (110) steps on the more open face, Au(410), is consistent with the above trends given the longer distance across each step, 8.5 Å.

A notable feature of the faces in the $[0\bar{1}1]$ as well as $[\bar{1}10]$ zones examined here is the observed occurrence of substantial surface relaxation and/or reconstruction at negative electrode charges. While a detailed examination of potential- (and hence charge-) dependent structure was not undertaken, this qualitative observation is similar to the well-known reconstructions of low-index gold electrodes which occur in the presence of small negative (and perhaps near-zero positive) electrode charges[1-10]. The charge-induced restructuring of Au(110) appears to be analogous to the well-known reconstruction of some (110) surfaces induced by alkali-metal adsorption in uhv[42]. A broadbased understanding of this phenomenon is as yet lacking[43], although several theoretical treatments for (110) surface have appeared[44-46]. The observed occurrence of the surface relaxations increasingly towards negative charges for

the present stepped faces may be rationalized by a simple electrostatic argument. The monoatomic steps yield an effective dipole, the positive pole pointing away from the metal, as a consequence of the anticipated diminution of electron density at the step atom. Surface relaxation involving buckling of the terrace, and depression of the step edge row should tend to decrease the surface dipole. Consequently, negative electronic charging of the metal surface, with the associated interfacial field thereby generated, will counteract this surface dipole and hence should help to stabilize the surface relaxation. Conversely, the application of a positive electronic charge (i.e. yielding a surface electron deficiency) should disfavor the occurrence of the surface relaxation. More generally, one might anticipate that the addition of electronic charge would encourage metal surface bonding. This is consistent with the occurrence of either surface relaxation or reconstruction under these conditions. The observation of "smoother" (i.e. smaller z-corrugation) atomic features on relaxed or reconstructed surfaces, mentioned above, is also suggestive of increased surface bonding associated with electronic delocalization at negative charges.

Of the various stepped faces examined here, only Au(331) undergoes a clearcut surface reconstruction at negative electrode charges, although the charge-induced relaxation for Au(311), for example, involves an apparently substantial change in the surface geometry. In the light of the foregoing discussion, the driving force for the (1 × 2) reconstruction observed on Au(311) may well originate from an attractive interaction between the row pairs (ca 4 Å apart) that are thereby formed (Fig. 3B). The absence of a related row-pairing reconstruction on Au(221) can be understood on this basis since a one-atom wider terrace would separate the row pairs by an additional 2 Å or so.

The comparison between the restructuring observed on Au(331) and Au(110) can insightfully be viewed on the basis of such row pairing. As already

mentioned, the latter (1 × 1) surface can be viewed as 2(111)–(111), thereby featuring one less atom across each (111) terrace than for Au(331). Similarly to the (1 × 2) rearrangement of Au(331), the (1 × 3) reconstruction observed for Au(110) requires only short-range lateral atomic motion. A key behavioral difference between reconstructed Au(331) and Au(110) is that a number of other surface microstructures are evident in the latter case. This structural variety probably arises in part from the ability of the atomic strings on the "symmetrically stepped" Au(110) surface to undergo *concerted* lateral motion[6], leading in particular to the creation of (1 × 2) islands as well as regions featuring wider unit cells. Formation of the (1 × 2) regions is likely driven by their stability versus the initially created (1 × 3) structure. It is worth mentioning that such differing Au(110) microstructures have not been reported previously. This is probably due to the severe paucity of atomic-resolution STM data: such structural variations will not be evident otherwise.

An interesting difference between the Au(331) and Au(110) surfaces concerns the domain-edge morphologies cutting across the $[1\bar{1}0]$ direction. As noted above, reconstruction of the former surface is accompanied by a marked diminution in the kink density; this can readily by understood on the basis of the attractive interactions between adjacent rows deemed responsible for the paired-row (1 × 2) structure. In contrast, the reconstructed Au(110) surface is characterized by a proliferation of such kinks (Fig. 9A, 10A), inferring little or no interaction between the adjacent rows. The major origin of such kinks on Au(110), however, probably lies in the occurrence of significant mass transport *along* the $[1\bar{1}0]$ direction so to transform initially (1 × 3) reconstructed regions into (1 × 2) domains by means of an "added-row" mechanism. Clear evidence for this mechanism is seen from the especially high density of (1 × 2) domains in lower-terrace regions close to highly kinked terrace steps (Fig. 9A).

The sharply contrasting behavior of Au(311) and Au(110) is also noteworthy in that the (1 × 1) structures are ostensibly quite similar, being 2(111)–(100) and 2(111)–(111), respectively. The observed presence of only surface relaxation, rather than substantial reconstruction, on Au(311) is perhaps surprising given the behavior of Au(110). The slightly longer (ca 0.8 Å) step-step distance, together with the asymmetric nature of the surface profile for Au(311) presumably favors the observed charge-induced relaxation, involving row pairing by mutual displacement of adjacent step and terrace rows (fig. 1, ref. 20).

4.2 *Significance to Other Interfacial Properties*

Given that the present STM results yield a level of local real-space structural detail for stepped gold surfaces which has been largely unavailable previously for either electrochemical or uhv systems, it is appropriate to consider briefly their consequences on a broader front. The present surfaces display a notable degree of uniform order on the nanoscale as well as local atomic level. While some local faceting can sometimes be observed, each of the surfaces display structures which are either close to those expected from a bulk termination, or involve surface relaxation or reconstruction so to yield a simple alteration of the unit cell.

This persistence of local order and retention of a largely uniform step morphology accounts for the success of such simple correlations as seen in Fig. 13 between E_{pzc} and the density of broken bonds d_{bb} anticipated for the (1 × 1) surfaces. The complete absence of hysteresis in the C_{dl}–E response for all stepped faces that do not exhibit charge-induced surface reconstruction is indicative of the stability of these surfaces in the presence of the substantial (ca 10^7 V cm^{-1}) electrostatic fields that typically are developed at metal-

solution interfaces. The contrasting occurrence of such C_{dl}-E hysteresis for the one stepped face, Au(331), seen to undergo reconstruction, along with its behavioral similarity to Au(110), points to the "plastic", rather than "elastic", nature of such charge-induced surface rearrangements.

Despite the broadbased significance of the issues involved, previous examinations of surface morphology as a function of the crystallographic orientation are few and far between. This is unsurprising, however, given the arduous nature of such studies, the difficulty in achieving *true* atomic resolution for highly corrugated surfaces using STM, and the limited information on local atomic order attainable from low-energy electron diffraction (LEED). Nevertheless, one previous systematic study for a number of stepped platinum faces in uhv using LEED[44] offers some useful comparison with the present results. By and large, the behavior of the present stepped gold surfaces is compatible with those for the corresponding clean platinum surfaces in uhv. It is noteworthy, however, that the resistance of the gold electrode surfaces to restructuring, especially faceting, appears at least as great as observed for platinum in uhv. Admittedly, most of the surfaces examined here are not vicinal in nature, for which faceting is expected to be most prevalent.

Nonetheless, despite a prediction to the contrary[48], there are now even more persuasive reasons than those apparent before the advent of atomic-resolution STM[23] to utilize high-index gold faces in exploring the influence of monoatomic steps and related structural features on surface electrochemical phenomena, including electrocatalytic processes[19]. To this end, however, it would clearly be desirable to explore the structure and stability of stepped gold surfaces in a wider range of electrochemical environments, including electrolytes featuring extensive specific adsorption. We plan studies along these lines for the near future.

Acknowledgements

This work is supported by the Office of Naval Research and the National Science Foundation.

REFERENCES

1) M.J. Weaver and X. Gao, Ann. Rev. Phys. Chem., 44 (1993), 459.

2) (a) X. Gao, A. Hamelin, and M.J. Weaver, Phys. Rev. Lett., 67 (1991), 618; (b) X. Gao, A. Hamelin, and M.J. Weaver, Phys. Rev. B, 46 (1992), 7096; (c) X. Gao and M.J. Weaver, Ber. Bunsenges Phys. Chem., 97 (1993), 507.

3) X. Gao, A. Hamelin, and M.J. Weaver, J. Chem. Phys., 95 (1991), 6993.

4) X. Gao, A. Hamelin, and M.J. Weaver, Phys. Rev. B., 44 (1991), 10983.

5) (a) N.J. Tao and S.M. Lindsay, J. Appl. Phys., 70 (1991), 5141; (b) N.J. Tao and S.M. Lindsay, Surf. Sci., 274 (1992), L546.

6) O.M. Magnussen, J. Wiechers, and R.J. Behm, Surf. Sci., 289 (1993), 139.

7) B.M. Ocko, J. Wang, A. Davenport, and H. Isaacs, Phys. Rev. Lett., 65 (1990), 1466.

8) J. Wang, B.M. Ocko, A. Davenport, and H. Isaacs, Phys. Rev. B., 46 (1992), 10321.

9) B.M. Ocko, G. Helgensen, B. Schardt, J. Wang, and A. Hamelin, Phys. Rev. Lett., 69 (1992), 3350.

10) I.M. Tidswell, N.M. Markovic, C.A. Lucas, and P.N. Ross, Phys. Rev. B, 47 (1993), 16542.

11) X. Gao and M.J. Weaver, J. Phys. Chem., 97 (1993), 8685.

12) X. Gao, G.J. Edens, A. Hamelin, and M.J. Weaver, Surf. Sci., 296 (1993), 333.

13) O.M. Magnussen, J. Hotlos, R.J. Behm, N. Batina, and D.M. Kolb, Surf. Sci., 296 (1993), 310.

14) M. Salmeron, B. Marchon, S. Ferrer, and D.S. Kaufman, Phys. Rev. B., 35 (1987), 3036.

15) C. Ocal, A.L. Vazquez de Parga, J. Alvarez, and S. Ferrer, J. Microscopy. 152 (1988), 697.

16) M. Borbonus, O. Haase, R. Koch, and K.H. Rieder, Vacuum. 41 (1990), 321.

17) M. Borbonus, R. Koch, O. Haase, and K.H. Rieder, Surf. Sci., 249 (1991), L317.

18) R. Koch, M. Borbonus, O. Haase, and K.H. Rieder, Appl. Phys. A, 55 (1992), 417.

19) A. Hamelin, Y. Ho, S-C. Chang, X. Gao, and M.J. Weaver, Langmuir, 8 (1992), 975.

20) X. Gao, A. Hamelin, and M.J. Weaver, Surf. Sci., 274 (1992), L588.

21) R.R. Adzic, M.W. Hsiao, E.B. Yeager, and G. Pruett, Surf. Sci., 273 (1992), L425.

22) B. Lang, R.W. Joyner, and G.A. Somorjai, Surf. Sci., 30 (1973), 454.

23) A. Hamelin, in "Modern Aspects in Electrochemistry", Vol. 16, B.E. Conway, R.E. White, and J. O'M. Bockris, eds., Plenum, New York, 1985, Chapter 1.

24) H. Othani, C-T. Kao, M.A. Van Hove, and G.A. Somorjai, Prog. in Surf. Sci., 23 (1986), 155.

25) (a) P. Jiang, F. Jona, and P.M. Marcus, Phys. Rev. B, 35 (1987), 7952; (b) F. Jona and P.M. Marcus, in "The Structure of Surfaces II", J.F. van der Veen and M.A. Van Hove, eds., Springer, Berlin, 1988, p. 90; (c) P.M. Marcus, P. Jiang, and F. Jona, ibid, p. 100.

26) T. Gritsch, D. Coulman, R.J. Behm, and G. Ertl, Surf. Sci., 257 (1991), 297.

27) For a review, see: D.M. Kolb, in "Structure of Electrified Interfaces", J. Lipkowski and P.N. Ross, eds., VCH Publishers, New York, 1993, Chapter 3.

28) A. Hamelin, J. Electroanal. Chem., 142 (1982), 299.

29) (a) A. Hamelin, J. Chim. Phys., 88 (1991), 1453; (b) A. Hamelin, J. Electroanal. Chem., 329 (1992), 247.

30) A. Hamelin, L. Stoicoviciu, G.J. Edens, X. Gao, and M.J. Weaver, J. Electroanal. Chem., in press.

31) X. Gao, A. Hamelin, and M.J. Weaver, to be published.

32) J.K. Mackenzie, A.J.W. Moore, and J.F. Nichols, J. Phys. Chem. Solids, 23 (1962), 185.

33) R. De Levie, J. Electroanal. Chem., 280 (1990), 179.

34) J. Lecoeur, J. Andro, and R. Parsons, Surf. Sci., 114 (1981), 320.

35) A. Hamelin and L. Stoicoviciu, J. Electroanal. Chem., 234 (1987), 93.

36) A. Hamelin, J. Electroanal. Chem., 210 (1986), 303.

37) A. Hamelin, X. Gao, and M.J. Weaver, J. Electroanal. Chem., 323 (1992), 361.

38) K.D. Hammonds and R.M. Lynden-Bell, Surf. Sci., 278 (1992), 437.

39) N.C. Bartelt, J.L. Goldberg, T.L. Einstein, and E.D. Williams, Surf. Sci., 273 (1992), 252.

40) E.H. Conrad, Prog. Surf. Sci., 39 (1992), 65.

41) S.P. Chen and A.F. Voter, Surf Sci., 244 (1991), L107.

42) R.J. Behm, in "Physics and Chemistry of Alkali Metal Adsorption", H.P. Bonzel, A.M. Bradshaw, and G. Ertl, eds., Elsevier, 1989, p. 111.

43) P.A. Thiel and P.J. Estrup, in "CRC Handbook of Surface Imaging and Visualization", A.T. Hubbard, ed., CRC Press, in press.

44) K-M. Ho and K.P. Bohnen, Phys. Rev. Lett., 59 (1987), 1833.

45) C.L. Fu and K-M. Ho, Phys. Rev. Lett., 63 (1989), 1617.

46) A.A. Kornyshev and I. Vilfan, Phys. Rev. B, 47 (1993), 10775.

47) D.W. Blakely and G.A. Somorjai, Surf. Sci., 65 (1977), 419.

48) P.N. Ross, in "Structure of Electrified Interfaces", J. Lipkowski and P.N. Ross, eds., VCH Publishers, New York, 1993, Chapter 2.

FIGURE CAPTIONS

Figure 1

Unit-cell ball models, and position on projected stereographic triangle, for surfaces studied here.

Figure 2

A) Unfiltered height-shaded STM image of Au(331) in 0.1 M $HClO_4$ at 0.2 V vs. SCE.

B) Close-up of region towards top right-hand corner of A.

Figure 3

Schematic side-view ball models illustrating

A) surface relaxation.

B) (1 × 2) surface reconstruction observed for Au(331).

Figure 4

A) Large-scale STM image of Au(331) at -0.3 V, showing (1 × 2) reconstruction.

B) Close-up image, showing "paired-row" structure of Au(331)-(1 × 2).

Figure 5

A) Atomic-resolution STM image of Au(221) at -0.2 V.

B) Large-scale image of Au(221) at 0 V, showing random domain edges with extended kinks.

Figure 6

Large-scale STM image of Au(533) at 0.2 V, showing random extended kinks.

Figure 7

A) Large-scale STM image of Au(210) at 0 V.

B) Close-up image of Au(210), showing local atomic order.

Figure 8

STM image of Au(410) at -0.1 V.

Figure 9

A) Large-scale STM image of reconstructed Au(110) at -0.3 V.

B) Atomic-resolution image of Au(110), showing differing string microstructures.

Figure 10

A,B) Similar to Figure 9, but showing microstructures consistent with conventional "missing-, added-row" configuration for Au(110).

Figure 11

A,B) Further atomic-resolution images of reconstructed Au(110) showing different string microstructures.

Figure 12

A-C) Double-layer capacitance - electrode potential curves for gold surfaces indicated in 10 mM $HClO_4$ during positive- and negative-going potential sweeps at 5 mV s^{-1}. Capacitance (y-axis) scale refers to bottom curves in each case, the two upper traces being shifted upward by 10 and 25 $\mu F\ cm^{-2}$ (A), 15 and 25 $\mu F\ cm^{-2}$ (B), and 15 and 25 $\mu F\ cm^{-2}$ (C) for clarity.

Figure 13

Plot of potential of zero charge, as estimated from the potential of the diffuse-layer capacitance minimum, E_{min}, for various high-index faces studied here (right-hand axis) versus the crystallographic angle for the (110) surface (circles). Curve is plot on common axis of "density of broken bonds" for ideal-bulk-termination surface, d_{bb}, (left-hand axis) estimated as outlined in refs. 32 and 33. Values of d_{bb} and E_{min} are scaled on y-axis by forcing the plots to coincide for Au(111) and (110). For faces where C_{dl}-E hysteresis is observed, E_{min} values refer to negative-going potential sweeps. Value for Au(100) obtained from ref. 37; for Au(111) from ref. 35 (see text).

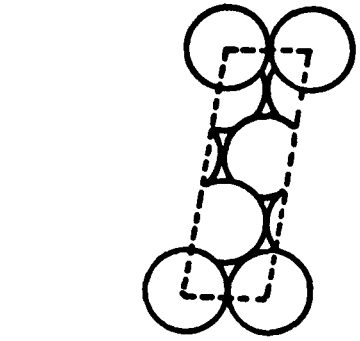

(533)=4(111)-(100)

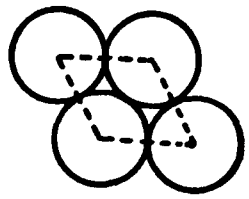

(111)

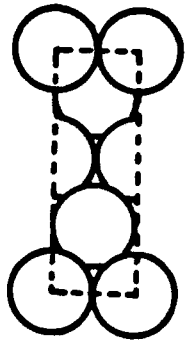

(221)=4(111)-(111)

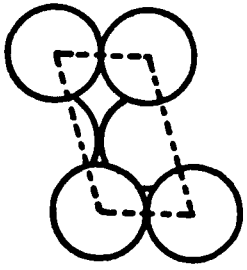

(311)=2(111)-(100)

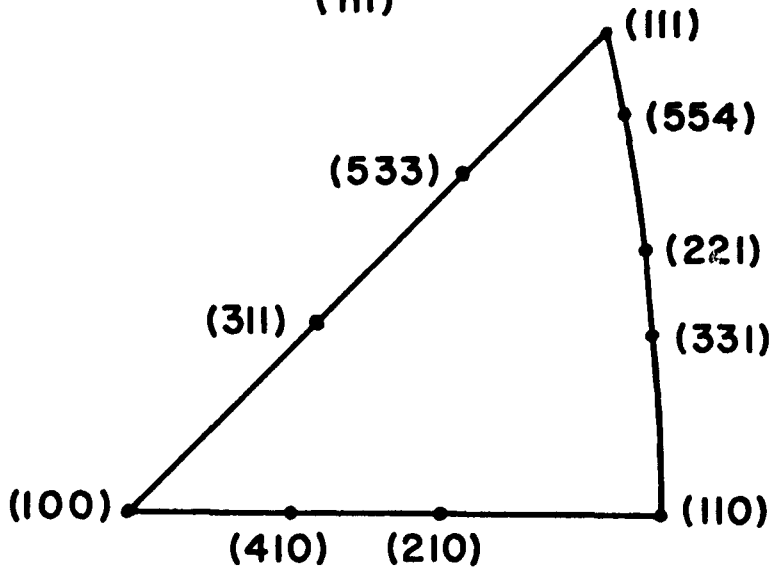

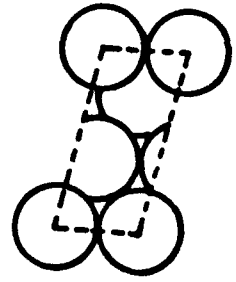

(331)=3(111)-(111)

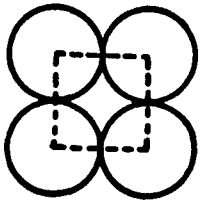

(100)

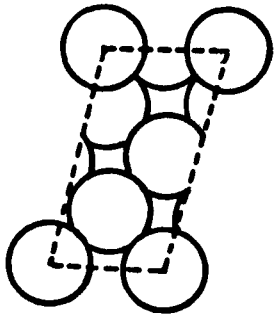

(410)=4(100)-(110)

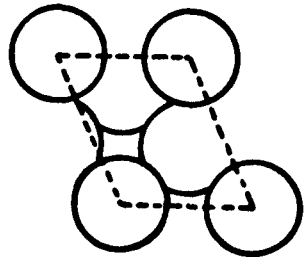

(210)=2(100)-(110)

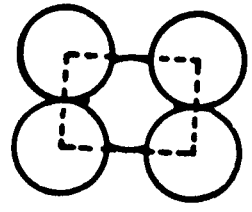

(110)

FIG 1

B

A

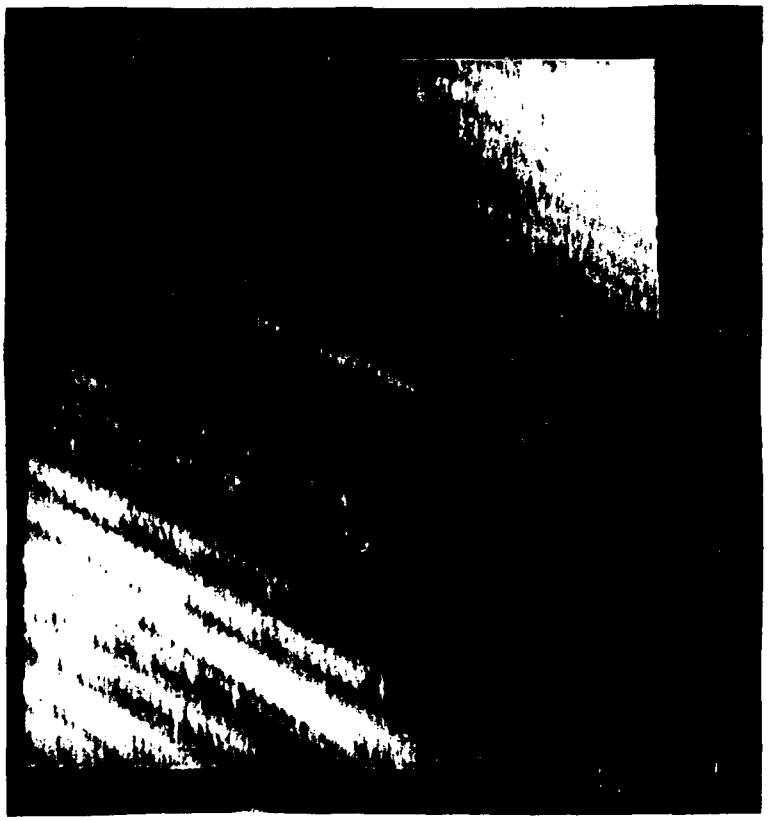

FIG 2

A

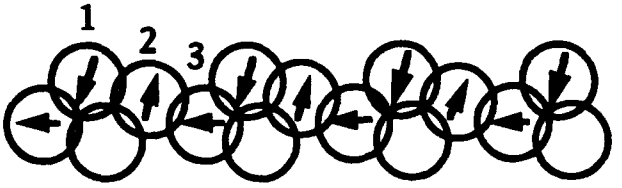

Side view of Au(331) relaxation

B

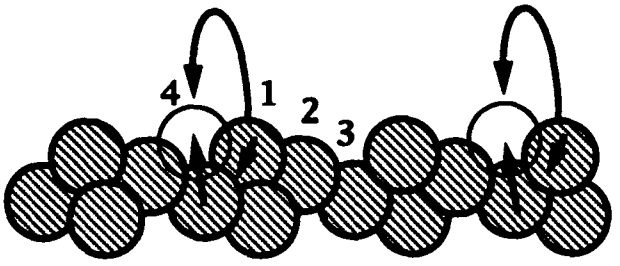

Side view of Au(331) (1x2) reconstruction

FIG 3

B

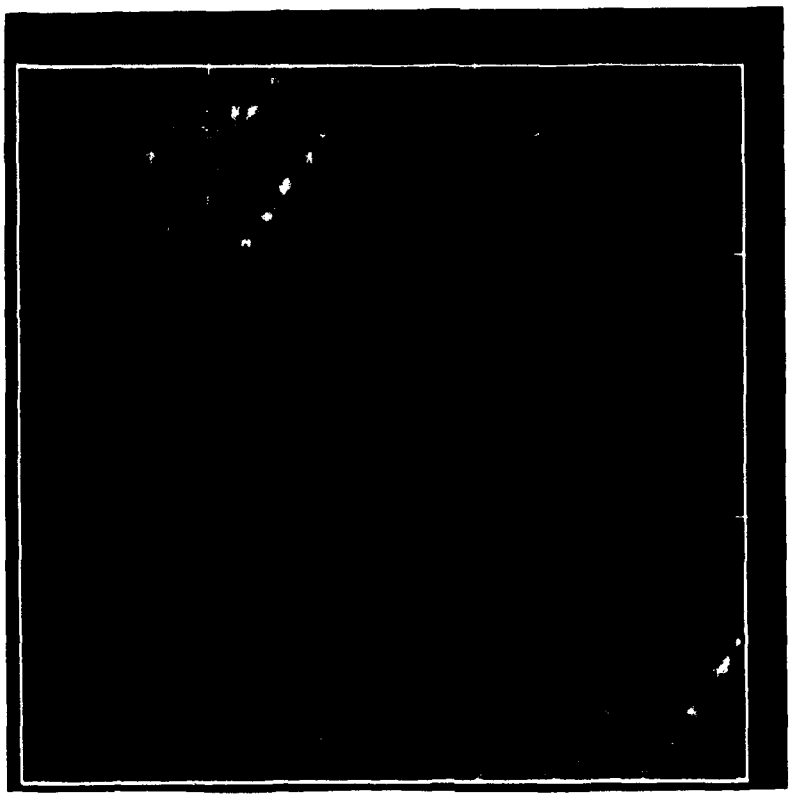

A

FIG 4

B

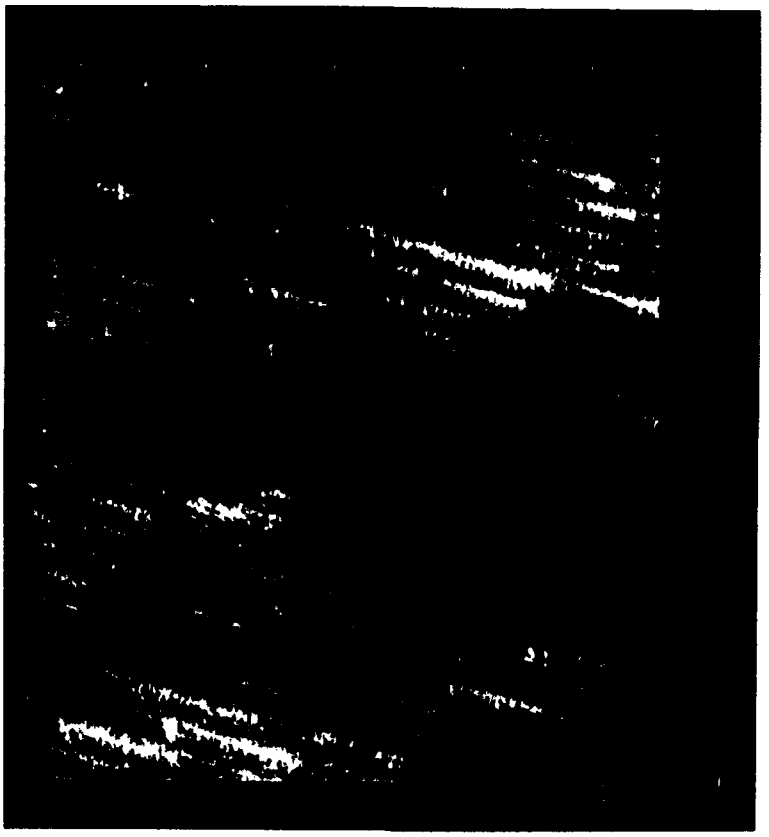

A

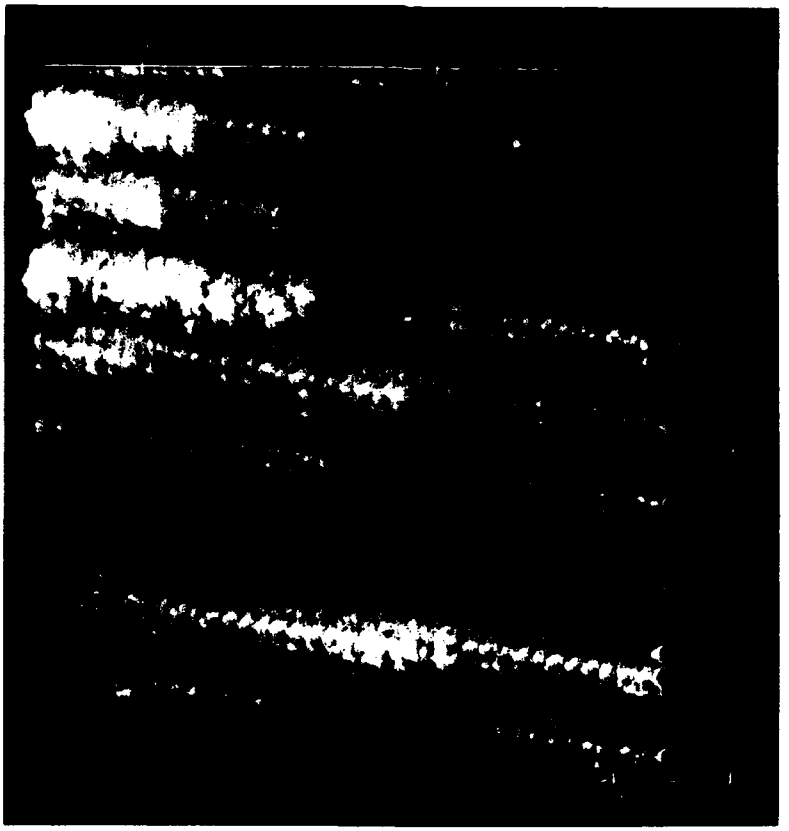

FIG 5

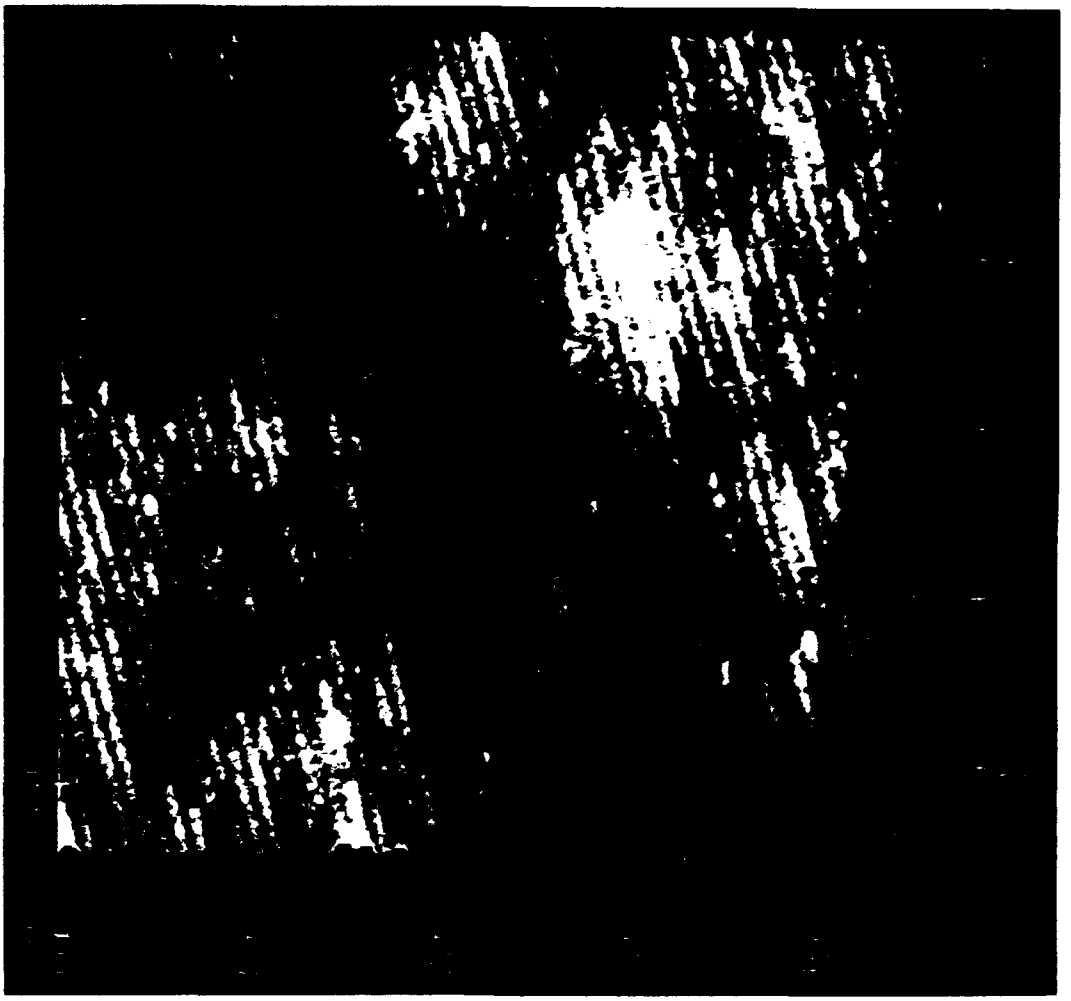

FIG 6

B

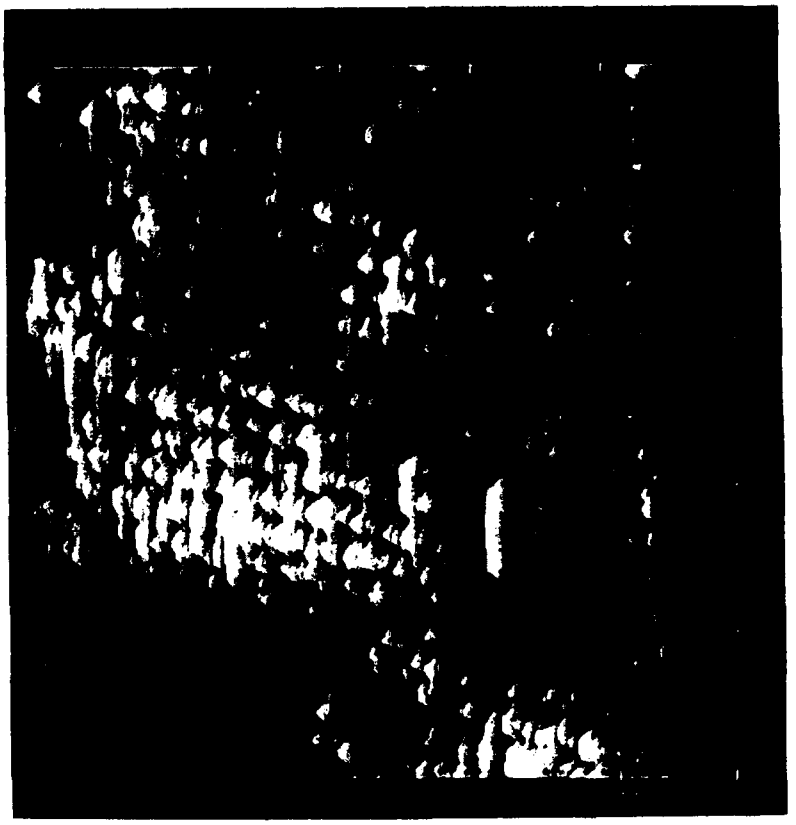

A

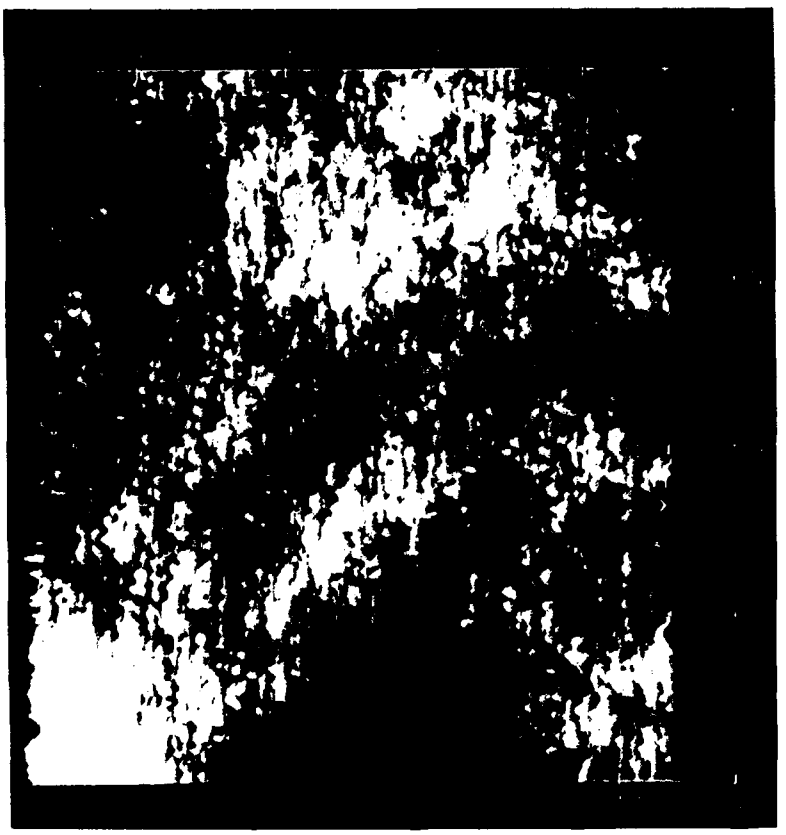

FIG 7

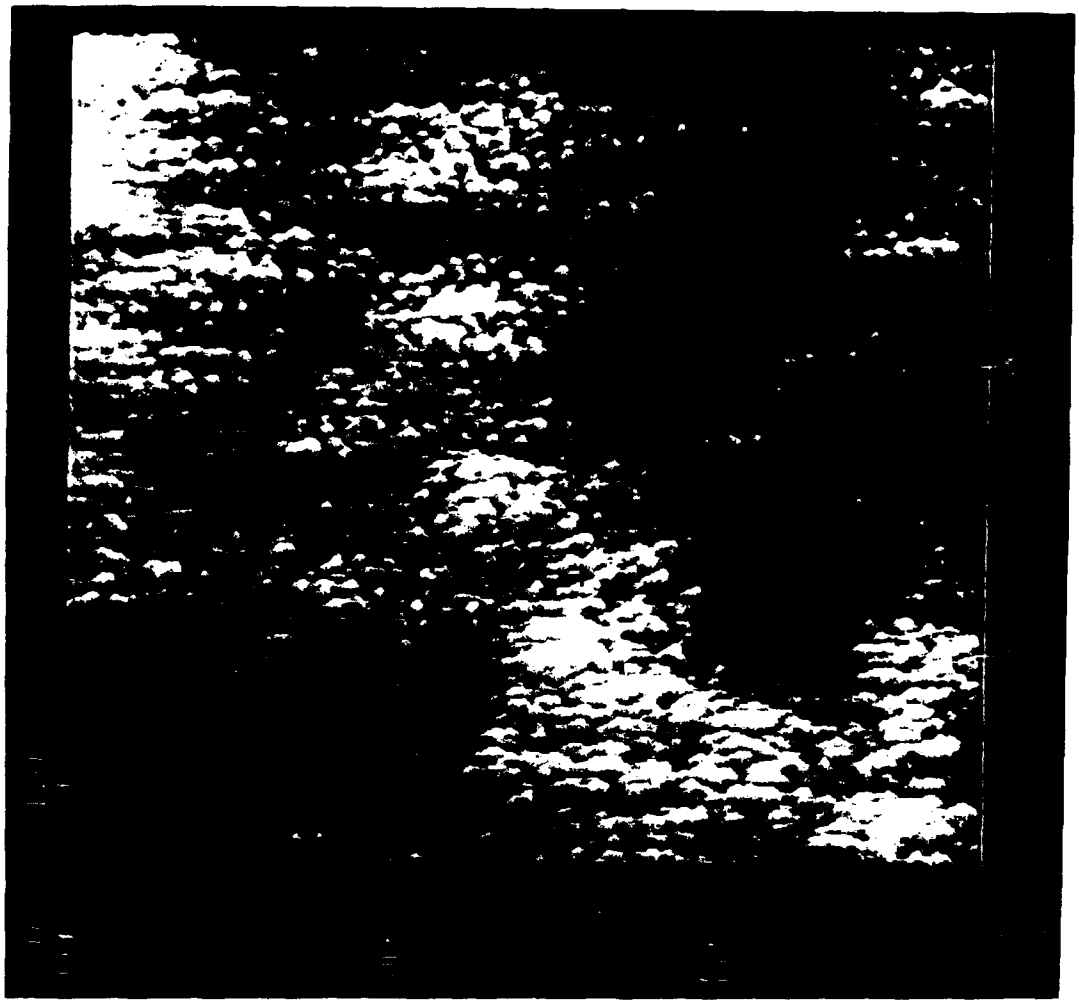

FIG 8

B

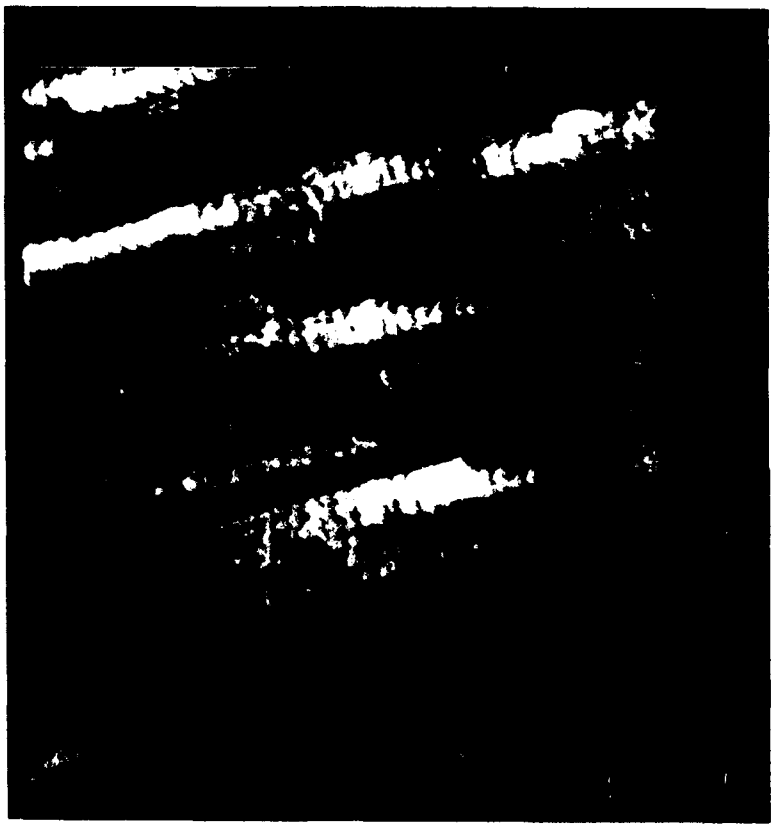

A

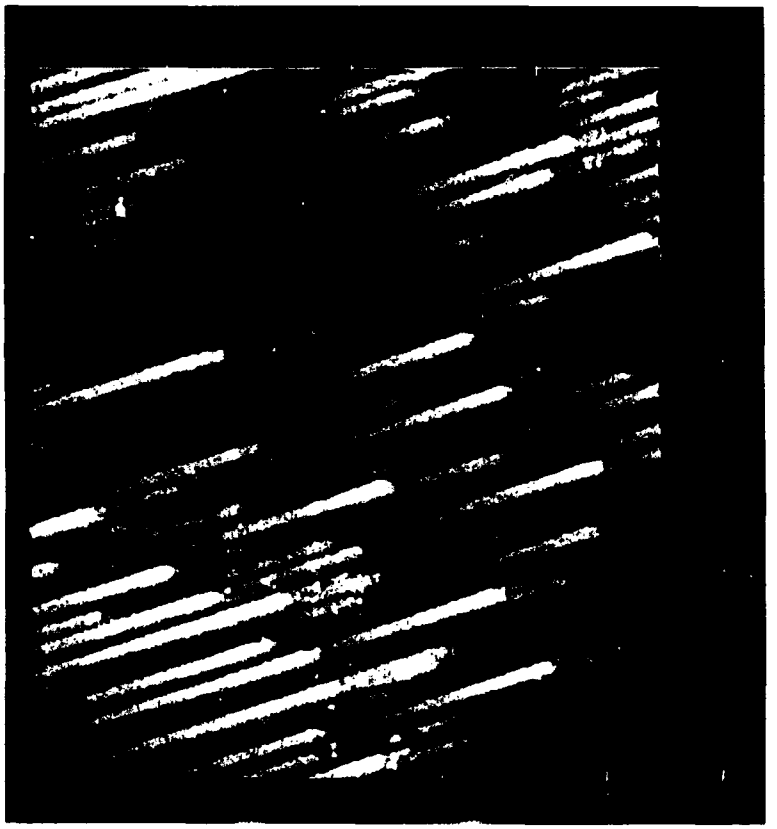

FIG 9

B

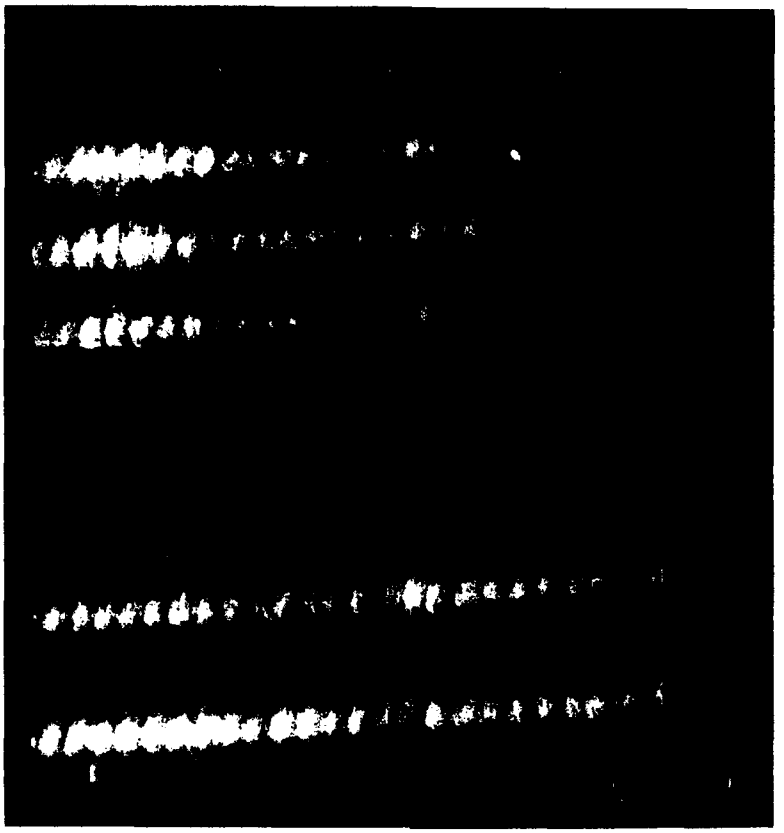

A

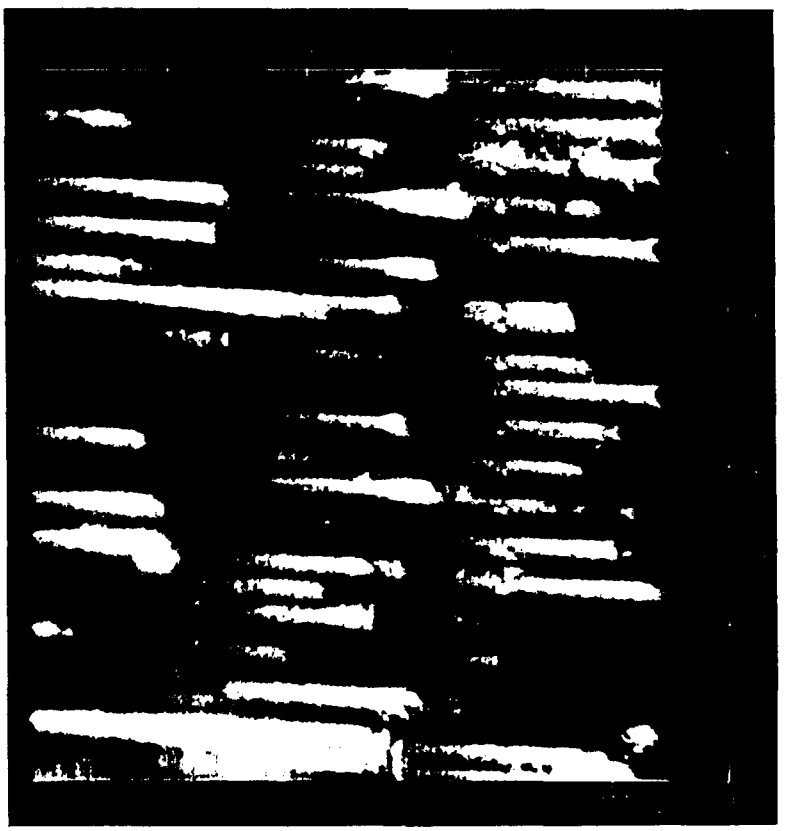

FIG 10

B

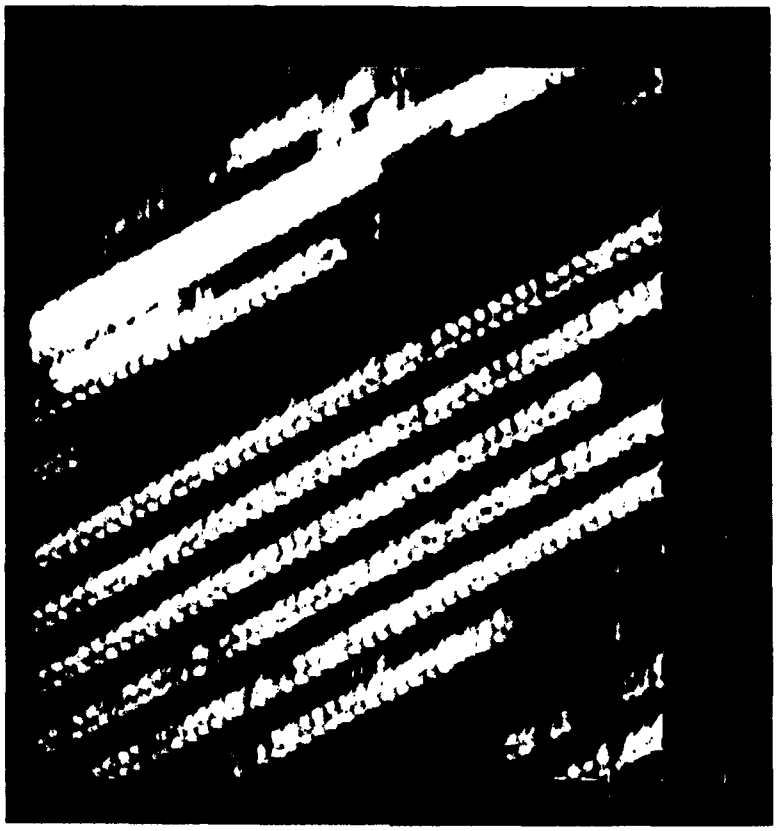

A

FIG 11

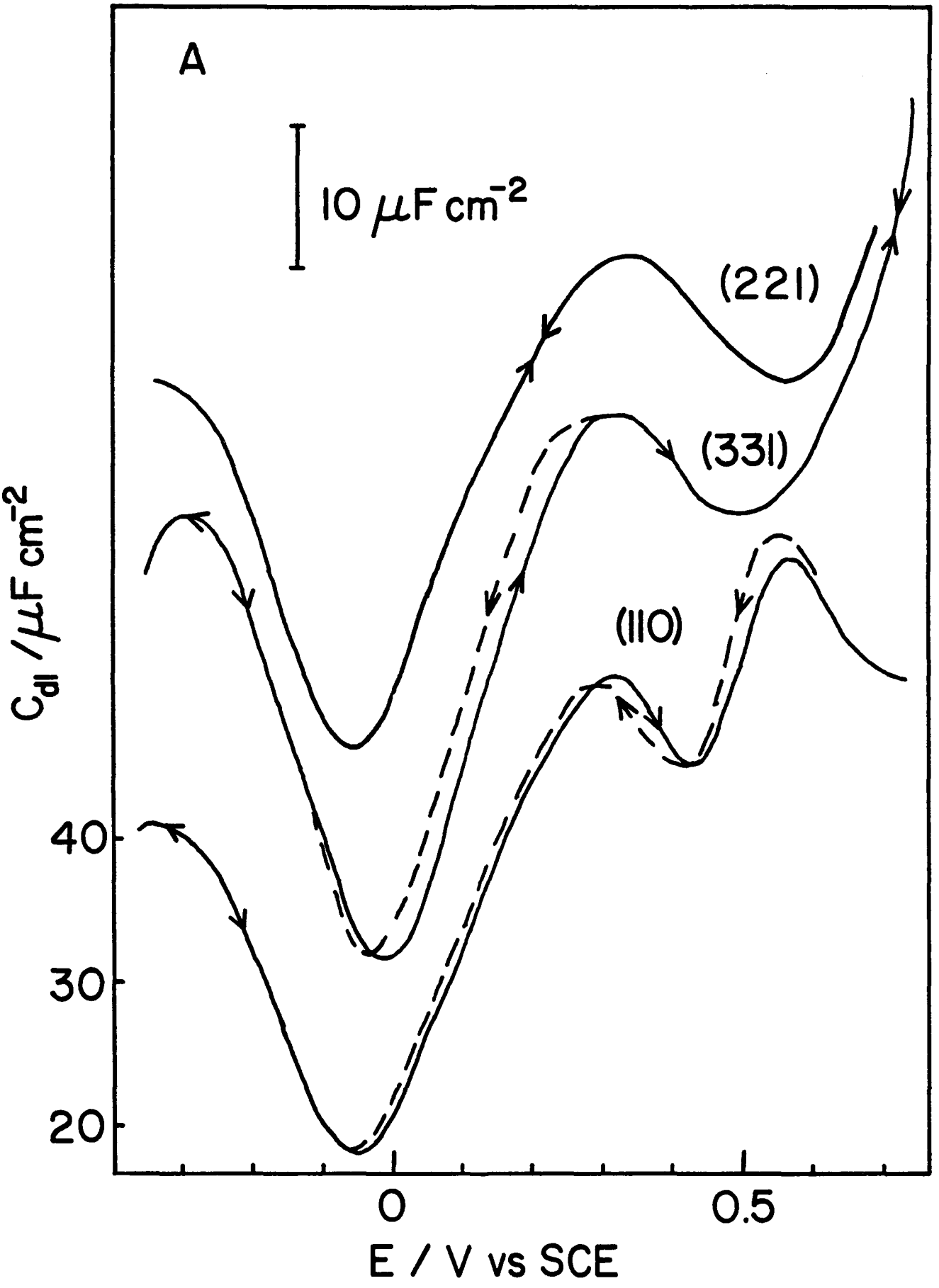

FIG 12A

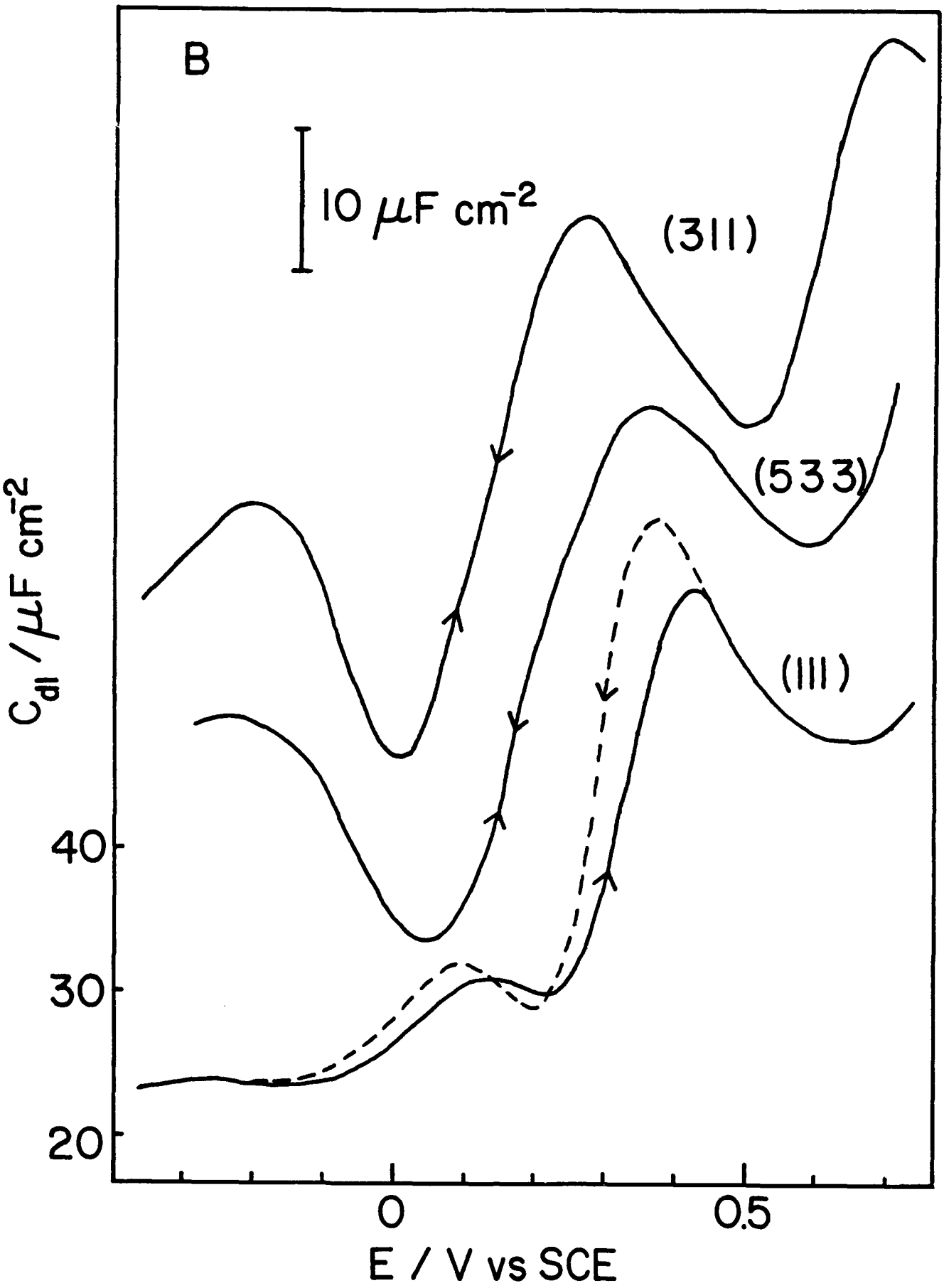

FIG 12B

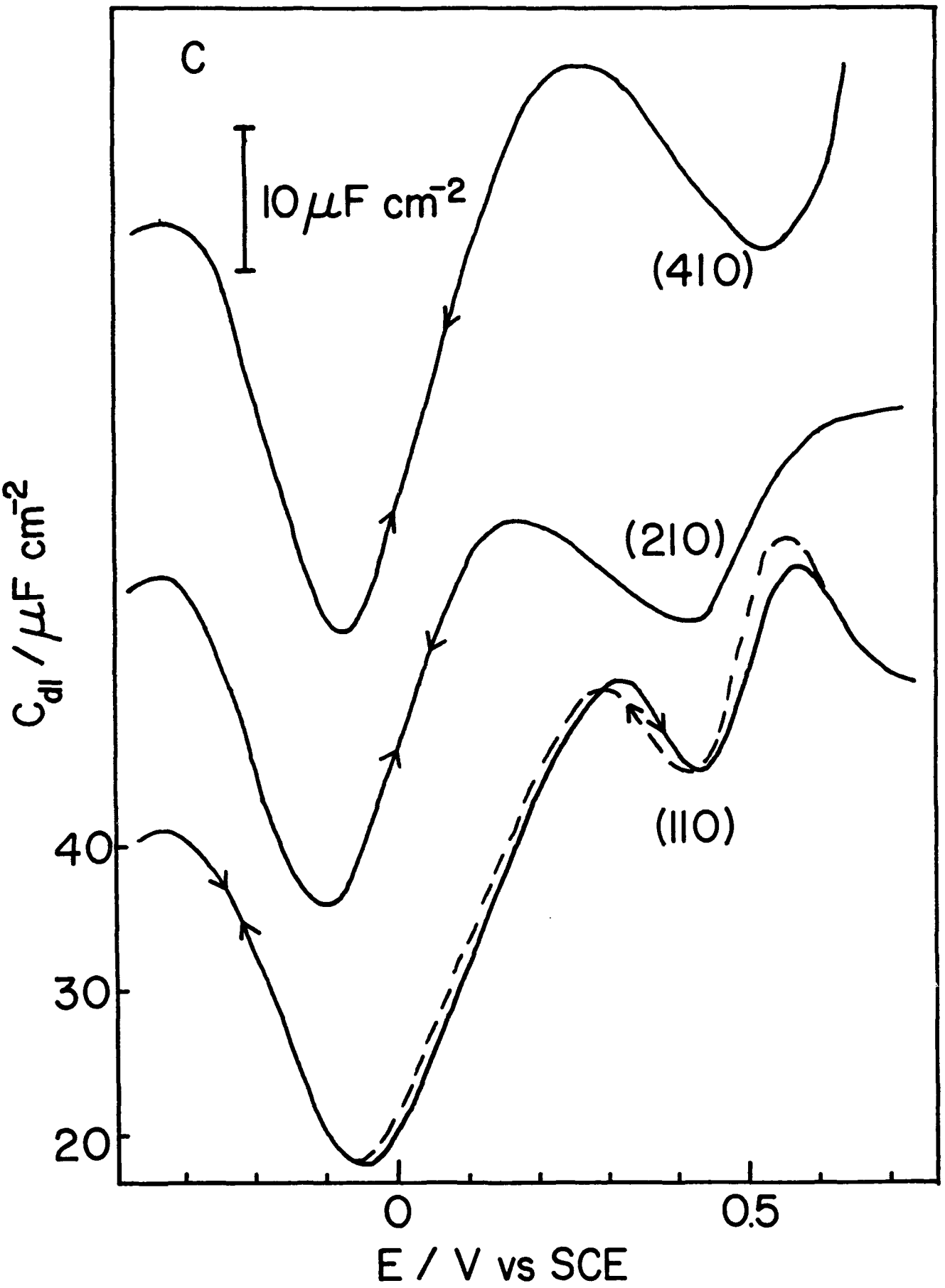

FIG 12C

d_{bb}
7.0
8.0
9.0
E_{min} / V vs SCE
0.4
0.2
0.0
-.2
0
40
80
120
degrees
(110)
(331)
(221)
(111)
(533)
(311)
(100)
(410)
(210)
(110)

FIG 13